Bearing capacity analysis of reinforced concrete L-shaped cross-section under biaxial eccentric compression*

JIAO Junting**, YE Yinghua and DIAO Bo

(Department of Civil Engineering, Beijing University of Aeronautics and Astronautics, Beijing 100083, China)

Received November 26, 2002; revised January 20, 2003

Abstract The ultimate capacity of short L-shaped reinforced concrete (RC) members subjected to biaxial eccentric compression is investigated to provide a new tool for structure engineers. On the basis of nonlinear analysis of RC arbitrary cross-section, a new simplified cross-section numerical integration method is suggested. The cross-section is divided into several triangles, and each one is integrated with Gauss integration method. And L-shaped cross-sections subjected to biaxial eccentric compression are analyzed. The interaction curves of $(N-M)$ and (M_y-M_z) for L-shaped sections are derived. The analytical results are well consistent with the experimental data and other analytical results.

Keywords: nonlinear analysis, L-shaped cross-section, biaxial eccentric compression, bearing capacity.

The ultimate capacity of irregularly shaped reinforced concrete members under biaxial eccentric compression is a complicated problem and necessary to be solved in present structure design. Because of biaxial eccentric compression, the neutral axis of a cross-section is not commonly vertical to the plane acted by bending moments and not parallel to edges of the cross-section. However, the neutral axial location is variable with the difference of cross-section dimension, reinforcement ratio, loading type and concrete strength. Because the calculation of the neutral axial location is complicated, and the manual calculation is bothersome, people have to use computers to do it. Now the calculation methods with computers mainly include strip method and rectangle method, which achieve the calculation by dividing the cross-section into strips or rectangles. Both the two methods may precisely calculate the ultimate capacity of a cross-section, but need more computing time.

A new simplified numerical integration method for the arbitrary cross-section is suggested here, which divides an arbitrary cross-section into several triangles, and each triangle is integrated with Gauss integration. The ultimate capacities of the arbitrary cross-section are analyzed. The interaction curves of $(N-M)$ and (M_y-M_z) for L-shaped RC cross-section under biaxial eccentric compression are derived. The calculation needs less computer time, and calculation results are precise. In addition, the method may also be applied to other structure analysis, such as steel-concrete composed structures.

1 Basic assumption and material properties

In the analysis, the basic assumptions and material properties used include:

(i) Sections remain plane after deformation.

(ii) The reinforcement is subjected to the same variations in strain as the adjacent concrete.

(iii) Shear deformation is ignored.

(iv) The tensile strength of concrete is ignored.

(v) The relationship between stress-strain distributions in concrete is assumed to be parabolic as illustrated by Fig. 1, in which σ_c, ε_c denote the stress and strain of concrete respectively, f_c is the design value of concrete column compressive strength. The ultimate compressive strain ε_{cu} at the highly compressed fiber is taken as -0.0033. The strain ε_0 at the maximum compressive stress is taken as -0.002. The stress σ_c is taken as $f_c\left[\frac{2\varepsilon_c}{\varepsilon_0}-\left(\frac{\varepsilon_c}{\varepsilon_0}\right)^2\right]$ when ε_c is greater than ε_0(see Fig. 1).

(vi) The stress-strain relation of reinforcement steel is taken as idealized elastic-plasticity (see

* Supported by the National Natural Science Foundation of China (Grant. Nos. 50178008 and 59978004)

** To whom correspondence should be addressed. E-mail: ylc@jyu.edu.cn

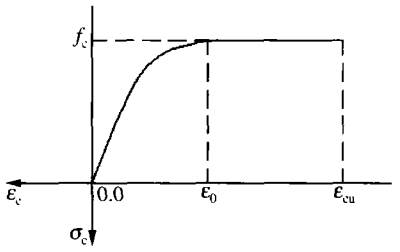

Fig. 1. Stress-strain curve of concrete.

Fig.2), where ε_s and σ_s are the strain and stress values of steel respectively, the strain ε_s is equal to f_y/E_s, f_y and E_s are the yield strength and the elastic modules of steel. The ultimate strain ε_{su} is 0.01.

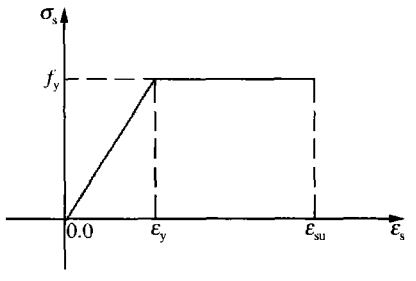

Fig. 2. Stress-strain curve of reinforcement.

2 Method of analysis

In the analysis, the coordinates of the biaxial eccentric load are indicated by y_n and z_n.

2.1 The strain of any point in a section

According to plane assumption, the strain ε at any point in a section is

$$\varepsilon = \varepsilon_0 + z\theta_y - y\theta_z = \boldsymbol{y}^T\tilde{\varepsilon}, \quad (1)$$

where ε_0, θ_y and θ_z are the strain at the origin of section coordinate system, curvature around y-axis and curvature around z-axis respectively, and $\boldsymbol{y}^T = [1 \quad z \quad -y]$, $\tilde{\varepsilon} = [\varepsilon_0 \quad \theta_y \quad \theta_z]^T$.

2.2 Equilibrium equations of section forces

The equilibrium equations of an arbitrary cross-section can be written as follows:

$$\boldsymbol{P} = \boldsymbol{D}_s\tilde{\varepsilon}, \quad (2)$$

$$\Delta\boldsymbol{P} = \boldsymbol{D}_t\Delta\tilde{\varepsilon}. \quad (3)$$

Here $\boldsymbol{P} = [N \quad M_y \quad M_z]^T$, $\boldsymbol{D}_s = \boldsymbol{D}_{s(c)} + \boldsymbol{D}_{s(s)}$, $\tilde{\boldsymbol{\varepsilon}} = [\varepsilon_0 \quad \theta_y \quad \theta_z]^T$ and $\Delta\boldsymbol{P} = [\Delta N \quad \Delta M_y \quad \Delta M_z]^T$, $\boldsymbol{D}_t = \boldsymbol{D}_{t(c)} + \boldsymbol{D}_{t(s)}$, $\Delta\tilde{\boldsymbol{\varepsilon}} = [\Delta\varepsilon_0 \quad \Delta\theta_y \quad \Delta\theta_z]^T$. Eq. (3) is the incremental form of Eq. (2). N is normal force along x axis, M_y and M_z are the bending moment around y and z axes, $\boldsymbol{D}_s$ and $\boldsymbol{D}_t$ are the secant stiffness matrix and tangent stiffness matrix of the section (specific derivation from Refs. [2,4]), $\boldsymbol{D}_{s(c)}$ is the secant stiffness matrix of concrete and $\boldsymbol{D}_{s(s)}$ is that of reinforcement, $\boldsymbol{D}_{t(c)}$ and $\boldsymbol{D}_{t(s)}$ express the tangent stiffness matrix of concrete and reinforcement, respectively.

2.3 Integration of cross-section stiffness

In the calculation, the stress and strain for materials are considered to be positive with tensile and compression to be negative. In the function $\boldsymbol{D}_s = \boldsymbol{D}_{s(c)} + \boldsymbol{D}_{s(s)}$, the integration of the section stiffness includes concrete section term $\boldsymbol{D}_{s(c)}$ and reinforcement bar term $\boldsymbol{D}_{s(s)}$. The concrete stiffness is derived from the summation of triangle unit stiffness (shown in Fig.3), which divides the integrated section into several parts. The triangle unit stiffness is integrated by the Gauss numerical method (shown in Fig.4).

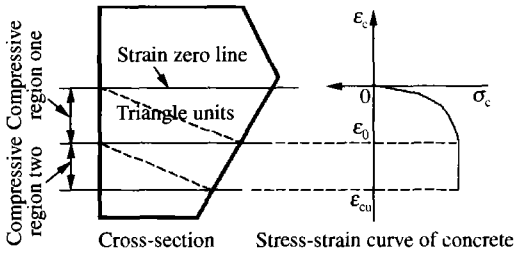

Fig. 3. Division of a cross-section.

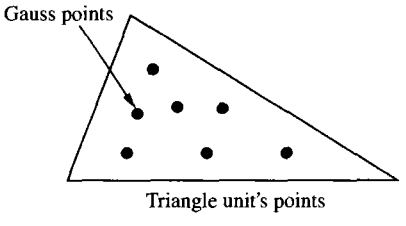

Fig. 4. Gauss points in one triangle unit.

3 Cross-section analysis

3.1 Analysis of cross-section and test data

Using the method expressed in this paper, the RC sections in Ref. [6] are calculated. The calculation results correspond well with the existing calculating results and experimental data of Ref. [6] (see Fig.5 and Table 1). The average value of the ratio $M'_{C,m}/M_{T,m}$ is 0.813. This shows that the analysis method derived in this paper is usable.

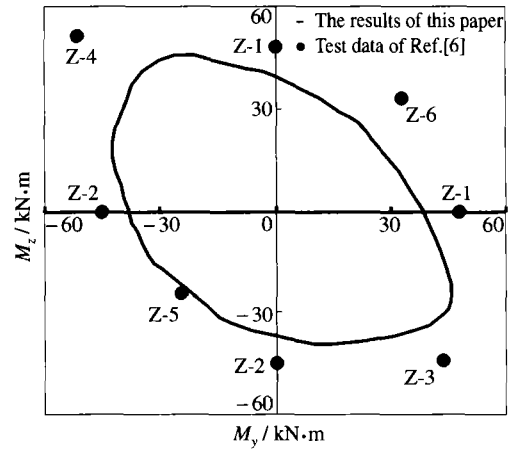

Fig. 5. Interaction curve of ($M_y - M_z$).

Table 1. Comparison between analysis results and test data

Specimen number	Experimental data		Theoretical data		
			Ref. [6]	This paper	
	N/kN	$M_{T,m}$/ kN·m	$M_{C,m}$/ kN·m	$M'_{C,m}$/ kN·m	$\frac{M'_{C,m}}{M_{T,m}}$
Z-1	220	47.96	38.33	38.51	0.803
Z-2	220	44.85	37.45	36.00	0.803
Z-3	220	62.10	48.06	48.63	0.783
Z-4	370	72.45	52.38	55.69	0.769
Z-5	220	34.50	33.47	33.98	0.985
Z-6	220	46.58	35.03	34.35	0.737

N, test axial compressive force; $M_{T,m}$, test ultimate bending moment; $M_{C,m}$, $M'_{C,m}$, theoretical ultimate bending moments.

3.2 Analysis of the L-shaped cross-section under bieccentric compression

RC L-section shown in Fig. 6 is analyzed as an example. The interaction curves ($N - M$) and ($M_y - M_z$) under constant normal axial compressive force are obtained. The influence factors of interaction curves ($N - M$) and ($M_y - M_z$) are analyzed.

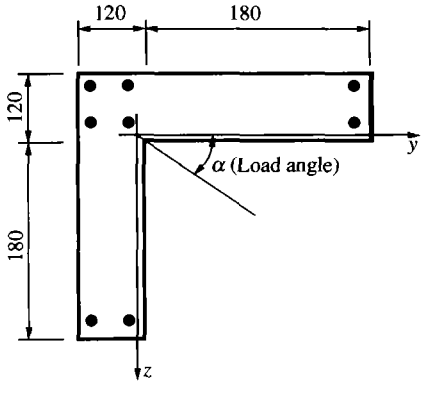

Fig. 6. L-shaped section.

3.2.1 Properties of ($N - M$) interaction curve

(i) Effects of the load angle $a = \mathrm{tg}^{-1}(M_y/M_z)$

Fig. 7(a) presents ($N - M$) interaction diagrams with different load angles but the same reinforcement ratio ($\rho = 1.00\%$) and concrete (C20). It shows that these ($N - M$) interaction diagrams are similar under eccentric compression, each curve is made up of two failure types: one is large eccentric failure, whose bending capacity increases with axial compression force up; the other is small eccentric failure, whose bending capacity decreases with axial compression force up. The limiting eccentric points of these diagrams vary with different load angles. The interaction diagram of 45° load angle is close to that of 225° load angle, and the area surrounded by this curve is the smallest, but the area surrounded by 135° curve is the largest, where the total moment M is $\sqrt{M_y^2 + M_z^2}$.

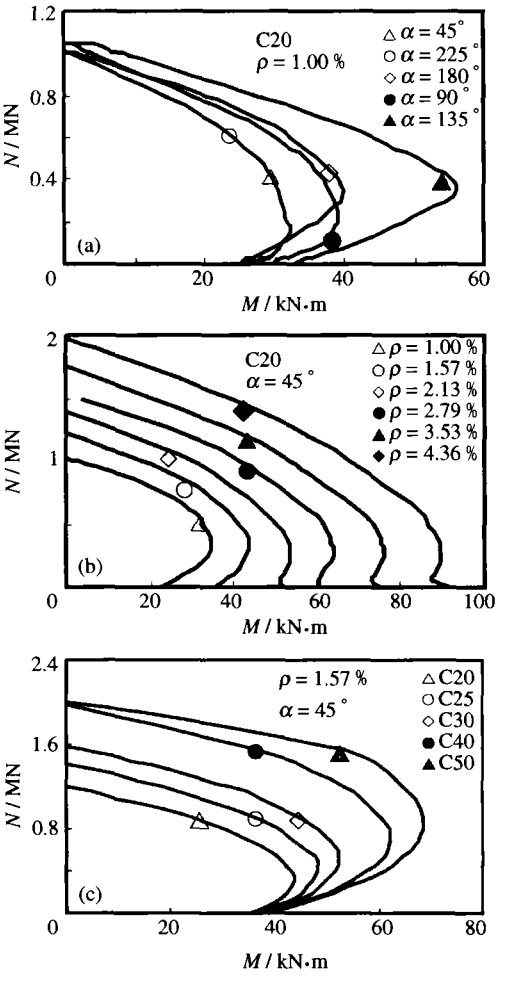

Fig. 7. Interaction curves of ($N - M$) with different load angles (a), reinforcement ratios (b) and concrete strengths (c).

(ii) Effects of reinforced ratio $\rho = A_s/A$

Fig. 7(b) shows ($N - M$) interaction diagrams with different reinforcement ratios but the same load angle ($\alpha = 45°$) and concrete (C20). When reinforcement ratio increases, the ultimate capacity rises, and the tendency is nearly linearly increasing with reinforcement ratio. The limiting eccentric points of these diagrams are almost irrelevant with reinforcement ratio.

(iii) Effects of concrete strength

Fig. 7(c) includes ($N - M$) interaction diagrams with different concrete strengths but the same load angle ($\alpha = 45°$) and reinforcement ratio ($\rho = 1.57\%$). It shows that the higher the concrete strength is, the larger its ultimate capacity is. For a small eccentric failure, if concrete strength is not greater than C40, the ultimate capacity changes linearly in accordance with the varieties of concrete strength. The limiting eccentric points of these diagrams are related with concrete strength, the higher the concrete strength is, the more upward the location of these points are.

3.2.2 Properties of ($M_y - M_z$) interactive curve

(i) Effects of axial compression ratio $\lambda = N/Af_c$

Fig. 8(a) illustrates ($M_y - M_z$) interactive diagrams with different axial compressive ratios λ but the same reinforcement ratio ($\rho = 1.00\%$), concrete (C20) and load angle ($\alpha = 45°$). When λ is small such as λ equal to 0 or $\lambda = 0.1286$ for a large eccentric failure, the interactive diagram looks like a revert triangle, with axial compressive ratio being up to the limiting value ($\lambda = 0.4501$), the interactive diagram turns gradually into an ellipse from the revert triangle, the area covered becomes larger. When axial compressive ratio continues to increase, the failure becomes small eccentric failure from a large eccentric failure, the interaction diagram turns gradually into a positive triangle from the ellipse, the area covered becomes smaller.

(ii) Effects of the load angle $a = \mathrm{tg}^{-1}(M_y/M_z)$

The ultimate bending capacity ($M = \sqrt{M_y^2 + M_z^2}$) of a section varies with different load angle. And the load angle at the biggest value of M is related to the axial compressive ratio (see Fig. 8 (a)).

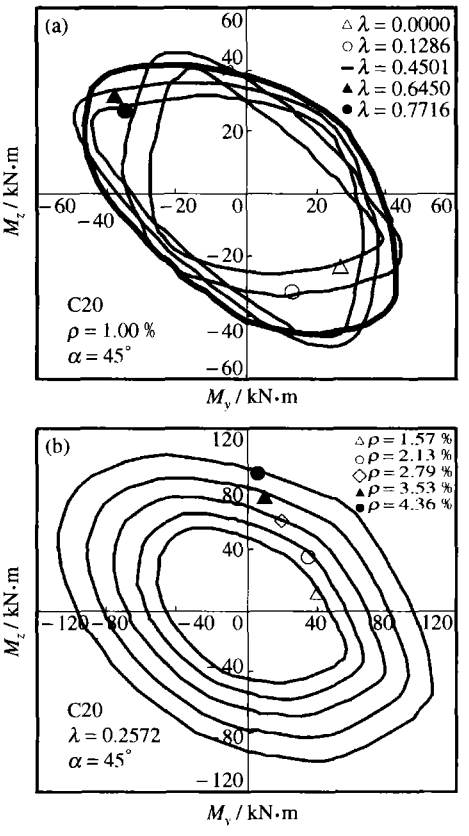

Fig. 8. The interaction curves of ($M_y - M_z$) with different axial compressive ratios (a) and reinforcement ratios (b).

(iii) Effects of reinforcement ratios $\rho = A_s/A$

Fig. 8(b) shows ($M_y - M_z$) interaction diagrams with different reinforcement ratios but the same axial compression ratio ($\lambda = 0.2572$), concrete (C20) and load angle ($\alpha = 45°$). It shows that the ultimate capacity M has a nearly linear relation with reinforcement ratio, while the reinforcement ratio does not affect the load angle at the biggest value of M.

4 Conclusions

(i) Based on the nonlinear analysis of RC arbitrary cross-section, a new simplified cross-section numerical integration method is suggested here. The cross-section is divided into several triangles, and each triangle is integrated with Gauss integration method.

(ii) L-shaped cross-sections subjected to biaxial eccentric compression are analyzed. The results well correspond with experimental data and other analytical results. It shows that the analysis method is correct and usable.

(iii) The interactive curves of ($N - M$) and ($M_y - M_z$) for the L-shaped sections are derived. The failure types under biaxial eccentric compression include large eccentric failure and small eccentric failure.

(iv) In the interactive diagrams of ($N - M$), load angle affects greatly the ultimate capacity of L-shaped section. At the load angles of 45° and 225°, the ultimate capacity is the least, and at 135°, the capacity is the largest.

(v) In the interactive diagrams of ($M_y - M_z$), the ultimate capacity increases with the increased axial compressive ratio for a large eccentric failure; and the ultimate capacity decreases with increasing of axial compressive ratio for a small eccentric failure; the capacity of limiting failure is variable with the axial compressive ratio, load angle, concrete strength and reinforcement ratio.

(vi) The method introduced in this paper is precise and needs less computing time. It may be extended to the arbitrary section with complex stress-strain distributions. It may also be applied to other section analysis such as analysis on steel-concrete composed structures.

References

1 Ye, Y. H. et al. Summary of nonlinear theory for reinforced concrete structures. Journal of Harbin Architecture & Civil Engineering Institute (in Chinese), 1995, (1): 127.

2 Ye, Y. H. et al. Nonlinear Analysis of Concrete Structures. Harbin: Harbin Institute of Technology Publishing House, 1996.

3 Ye, Y. H. et al. Nonlinear complete path analysis of reinforced concrete column with arbitrary cross-section. Journal of Harbin University of Architecture and Engineering (in Chinese), 1995, (5): 12.

4 Ye, Y. H. et al. Nonlinear stiffness matrix of cross-section of reinforced concrete beams under the combined loads of normal force, bending, shear and warping torsion. Journal of Harbin University of Architecture and Engineering (in Chinese), 1996, (2): 20.

5 Diao, B. et al. Strength analysis of reinforced concrete columns with arbitrary cross-section under bieccentric loadings. Progress in Natural Science, 2001, 11(4): 309.

6 Liu, C. et al. The experimental research on load-bearing capacity of L-shape members under axial compression and biaxial bending. Supplement of Engineering Mechanics (in Chinese), 1995, 0822.

7 Diao, B. et al. Nonlinear analysis of steel-concrete composite member under biaxial eccentric compression loading. Industrial Construction (in Chinese), 2002, (2): 44.

8 Wang, D. et al. Research on experiment and design method of specially shaped columns under eccentric loading. Journal of Building Structures (in Chinese), 2001, (5): 37.

9 Hsu, T. C. T-shaped reinforced concrete members subject to bending and axial compression. ACI Structural Journal, 1989, 86 (4): 460.

10 Yau, C. Y. Biaxial bending design of arbitrarily shaped reinforced concrete column. ACI Structural Journal, 1993, 90(3): 269.

11 Mallikarjiunal. Computer aided analysis of reinforced concrete columns subjected to axial compression and bending -I L-shaped sections. Computer and Structures, 1992, 44(5): 1121.

12 Dundar, C. Arbitrarily shaped reinforced concrete members subjected to biaxial bending and axial load. Computer and Structures, 1993, 49(4): 643.